Arabian Journal for Science and Engineering
https://doi.org/10.1007/s13369-025-10140-x

RESEARCH ARTICLE-ELECTRICAL ENGINEERING

Hepta-Band Ultra-Thin Metasurface Absorber for S-, C-, X-, Ku-, and K-Band Applications

Merve Kurt[1] · **Gokhan Ozturk**[1] · **Mehmet Ertugrul**[2]

Received: 20 November 2024 / Accepted: 11 March 2025

Abstract

This article presents a metasurface absorber demonstrating high absorption performance in the microwave range. The proposed absorber operates in the $S-$, $C-$, $X-$, $Ku-$, and $K-$band frequencies, achieving over 90% absorption at seven different frequency points. The peak absorption frequencies of the absorber are 2.8, 6.32, 9.17, 12.21, 14.4, 17.3, and 19.5 GHz, with absorption performances of 92.6, 91.7, 93, 96.3, 97.4, 98.3, and 99.8%, respectively. The metasurface is printed on an economical FR-4 substrate, and the unit cell size is designed to be very thin, measuring $0.146\lambda_o \times 0.146\lambda_o \times 0.0093\lambda_o$ in terms of the maximum wavelength. The design consists of four different resonators, each with a symmetric structure, which makes the design polarization insensitive for both transverse electric (TE) and transverse magnetic (TM) modes. When examining the absorber's performance at oblique angles, it was observed that, except for the third peak point, the other six peak points maintain absorption performance above 80% up to 45 degrees. At the third peak point, the absorption performance is around 65% at 45 degrees. To better understand the absorption mechanism, the characteristic impedance, permittivity, permeability, surface current, electric and magnetic field distribution graphs of each resonator were analyzed. To verify the reliability of the simulation results, the design's equivalent circuit model (ECM) was created using the ADS circuit simulator. The monostatic RCS of the design was investigated, and it was found to exceed 7 dBsm at the absorbing frequencies. Additionally, a prototype of the proposed special metasurface absorber was fabricated, and experimental absorption performance was obtained. The prototype measurement results were found to be quite consistent with the simulation results.

Keywords Metasurface · Absorber · Cost-effective bandwidth · Ultra-thin

1 Introduction

Today, the defense industry is rapidly adapting to advancing technology by developing metasurface absorber designs and devices. These devices are designed to minimize the traces of electromagnetic (EM) waves and provide invisibility to radar [1]. Metasurfaces are artificially manufactured materials whose properties can be altered according to their intended use, differing from naturally occurring materials. These special materials, commonly used in electromagnetic absorbers, have the capability to control electromagnetic waves [2]. Metasurface structures offer a wide range of functionalities due to their various methodological features. These structures can be effectively used as signal absorbers [3, 4] and polarization converters [5, 6], and they provide significant advantages in many areas such as antenna systems [7, 8], medical applications [9, 10], radar cross section reduction [11, 12], image processing [13–15], and sensor technologies [16–18]. Moreover, metamaterials that enable the manipulation of electromagnetic waves have also been developed for applications such as high-energy absorption systems [19], target detection and positioning [20], and wireless communication and data storage [21]. Metasurface absorber designs are typically structured in a metal–dielectric–metal configuration. In these designs, various materials such as FR-4

Merve Kurt and Gokhan Ozturk have contributed equally to this work.

✉ Merve Kurt
merve.kurt025@gmail.com

✉ Gokhan Ozturk
gokhan.ozturk@atauni.edu.tr

Mehmet Ertugrul
ertugrul@ktu.edu.tr

[1] Department of Electrical and Electronics Engineering, Ataturk University, Erzurum 25240, Turkey

[2] Faculty of Engineering, Department of Metallurgy and Materials Engineering, Karadeniz Technical University, Trabzon 61000, Turkey

Published online: 04 April 2025

[22, 23], Rogers [24], quartz [25], and polymer [26] are used as the dielectric layer. Unlike high-cost, hard-to-access, and complex-to-manufacture materials such as Arlon [27], F4B [28], and LCP[29], which are commonly used as substrates in microwave devices, FR4 material stands out due to its low cost, easy accessibility, compatibility with PCB technologies, and ease of manufacturing. It also offers high mechanical strength, making it a highly attractive choice. The primary goal of absorber designs is to prevent the reflection and transmission of the transmitted electromagnetic wave within the metal–dielectric–metal structure, thereby enabling wave absorption. This situation indicates that the impedance of the medium is matched with the free space impedance [30]. When physically examined, metasurface absorber designs can be created in single-layer [31, 32] or multi-layer [33, 34] structures. For an effective absorber design, it is important that the structures are compact and the materials used are cost-effective. Additionally, metasurface structures can operate across different frequency ranges, such as microwave, radio, optical, and ionizing radiation [35–37]. This diversity highlights the broad application potential and versatility of metasurfaces. Research on metasurfaces began in 2008 with Landy's high-performance design in the X-band [38] and has continuously evolved. Recent contributions to this development have been made by researchers including Saif Hannan with a four-band design in 2020 [39], Elakkiya with a five-band design in 2021 [40], Adnan Yousaf with a high-efficiency four-band design in 2022 [41], Laxmikant Dewangan with an effective three-band design in the K-band in 2023 [42], and Md. Golam Rabbani with a four-band design in 2024 [43]. Additionally, Md. Shakibul Hasan has worked on high-performance four-band absorption designs in the $S-$, $C-$, $X-$, and $Ku-$bands [44]. Recent research indicates an increasing interest in metasurface absorbers with higher numbers of bands and high absorption capacities while maintaining minimal sizes. These metasurfaces are expected to show high stability depending on the polarization state and incident angle of the electromagnetic waves. Accordingly, an ultra-thin, polarization-insensitive seven-band metasurface absorber has been designed. The presented FR-4 dielectric-based metasurface absorber is designed by integrating four resonators. This design provides effective absorption at a total of seven different frequencies in the $S-$, $C-$, $X-$, $Ku-$, and $K-$bands. With its unique structural design, this metasurface achieves absorption performances of 92.6, 91.7, 93, 96.3, 97.4, 98.3, and 99.8% at frequencies of 2.8, 6.32, 9.17, 12.21, 14.4, 17.3, and 19.5 GHz, respectively. The thickness of the design is set at $0.00093\lambda_o$, indicating a very thin structure. Due to its strong resonance characteristics, the absorber maintains an absorption performance of over 80% at oblique angles up to 45 degrees at six of the seven peak points, except for the third peak point, where the absorption performance is approximately 65% at 45 degrees. In terms of polarization insensitivity, the design shows similar absorption performance in both TE (transversal electric) and TM (transversal magnetic) modes, indicating its insensitivity to different polarization states. To support the accuracy of the study and the effectiveness of the design, detailed analyses of the design's characteristic impedance parameters, permittivity, permeability, electric, magnetic field distribution, and surface current were presented. To verify the reliability of the simulation results, the design's equivalent circuit model (ECM) diagram was created using the ADS (Advanced Design System) circuit simulator, and this model was compared with the S11 values obtained from simulations performed using CST Microwave Studio. The results show that both simulations consistently support each other. The monostatic RCS of the proposed design was examined to evaluate its absorption performance. Additionally, measurement results obtained from the prototype were compared with simulation results, and consistency was achieved across all results. This consistency validates the theoretical assumptions of the design and plays a crucial role in evaluating its real-world performance.

2 Design and Development

The unit cell structure of the proposed metasurface absorber and the locations of the geometric parameters are shown in Fig. 1a,b. In the proposed design, the bottom and top layers are made of copper with an electrical conductivity (σ) of 5.8×10^7 S/m, while the intermediate layer uses FR-4 dielectric material with an electrical permittivity $\epsilon_r = 4.3$, magnetic permeability $\mu_r = 1$, and loss tangent $tan\delta = 0.025$. The thickness of the copper layer is $t = 0.035$ mm, and the thickness of the FR-4 dielectric material is $h = 1$ mm.

In Fig. 1a,b, the dimension values of the unit cell structure of the proposed absorber are detailed in Table 1 in millimeters.

Figure 2 shows the absorption results of the proposed metasurface absorber simulated using CST Microwave Studio. As shown in Fig. 2, the proposed MS absorber achieved absorption rates of 92.6, 91.7, 93, 96.3, 97.4, 98.3, and 99.8% at resonance points for frequencies of 2.8, 6.32, 9.17, 12.21, 14.4, 17.3, and 19.5 GHz, respectively, in the S-, C-, X-, Ku-, and K-bands.

When examining the development process of the unit cell of the presented metasurface absorber, it has been determined that the integration of four different resonators leads to the basic absorbing structure. Figure 3a–d shows the designs of the hepta-band metasurface absorber consisting of four different resonators. Additionally, it has been concluded that the capacitive coupling effect between these four different resonators plays a critical role in achieving absorption during the design process. The integration of the resonators

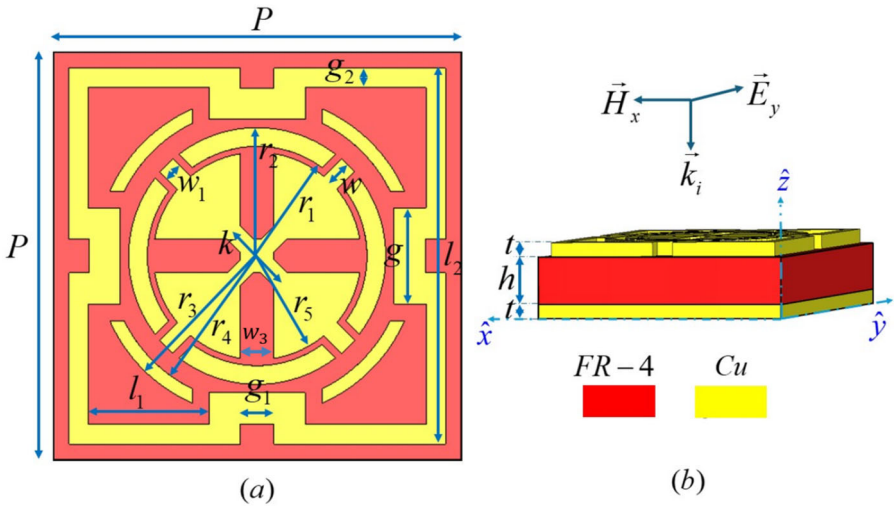

Fig. 1 Schematic view of the proposed MS-based absorber: **a** top view and **b** side view

Table 1 Parameter values of the proposed MMA in millimeters

$p = 15.7$	$g = 3.7$	$g_1 = 1.3$	$g_2 = 0.75$	$w = 0.97$	$w_1 = 0.7$	$k = 2.54$	$w_3 = 1.3$
$l_2 = 14.5$	$l_1 = 4.65$	$r_1 = 4.23$	$r_2 = 4.95$	$r_3 = 6.2$	$r_4 = 5.7$	$r_5 = 4$	$t = 0.035$

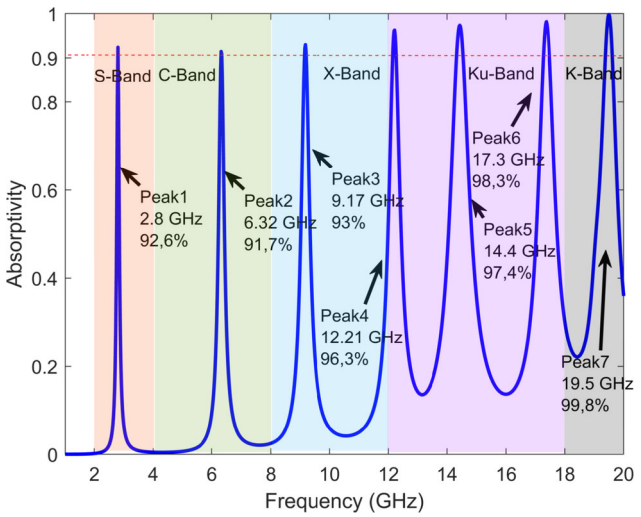

Fig. 2 Simulated absorption performance of the proposed metasurface absorber unit cell

increases the capacitance coupling, leading to the formation of new resonance frequencies and the appearance of new absorption peaks in the absorption spectrum. The new capacitance and inductance formed by these integrations result in strong resonances at different frequencies. Additionally, the new impedances created by the resonator integration lead to increased losses within the absorber[45].

In the proposed metasurface design, the varying geometries of four different resonators enable multi-band and frequency-selective absorption through electric and magnetic dipole resonances. The square resonator (Resonator 1) creates electric dipole resonance due to corner openings and edge structures, generating strong resonances at the 1st, 3rd, 5th, and 7th peaks. The cross resonator (Resonator 2) triggers both electric and magnetic dipole resonances, causing the electric field to concentrate in different directions, offering multi-band absorption at the 2nd, 6th, and 7th peaks. The ring resonator (Resonator 3) induces magnetic dipole resonance through circulating currents, producing strong resonances at the 4th and 7th peaks. The split-ring resonator (Resonator 4) combines both electric and magnetic dipole resonances, exhibiting resonance behavior at the 6th peak. As a result, electric dipole resonances are formed due to charge accumulation and the movement of the electric field in specific directions, while magnetic dipole resonances occur through circulating currents. In the square and cross resonators, electric dipole resonances dominate, whereas in the ring and split-ring resonators, magnetic dipole resonances are more pronounced. The combination of different resonators enables effective absorption across various frequency ranges. This structure creates the metamaterial performance through multi-band absorption characteristics resulting from the interactions between the resonators[45, 46].

Figure 4a–d shows the absorption performance of each resonator in the hepta-band metasurface absorber formed by the integration of four different resonators. Additionally, the graphs in Fig. 4a–d present the final absorption performance of the metasurface-based absorber, which is compared with the absorption results of each individual resonator.

Figure 4a shows that the first resonator of the proposed metasurface absorber exhibits absorption performances of

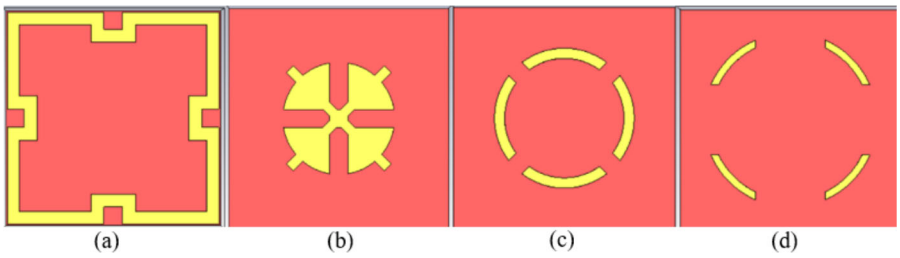

Fig. 3 Top view of the unit cell geometries for the hepta-band absorber composed of four different resonators: **a** Resonator 1, **b** Resonator 2, **c** Resonator 3, **d** Resonator 4

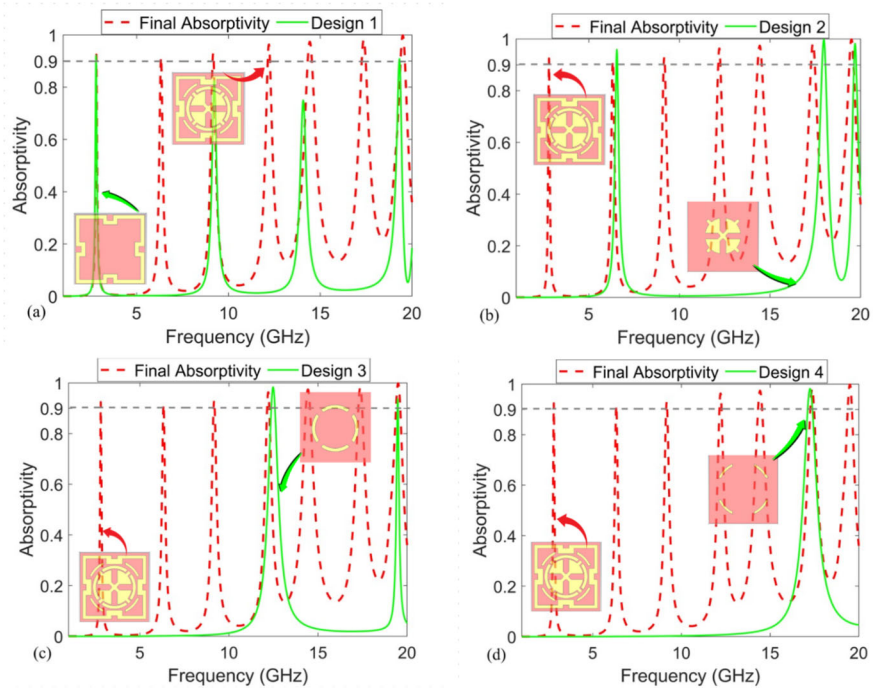

Fig. 4 Absorbance performances of **a** Resonator 1, **b** Resonator 2, **c** Resonator 3, **d** Resonator 4 constituting the proposed hepta-band MSA

92.3, 82.6, 74.9, and 90% at frequencies of 2.78, 9.2, 14.07, and 19.3 GHz, respectively. The graph in Fig. 4b reveals that the second resonator demonstrates performance in the C-, Ku-, and K-bands, achieving absorption rates of 96, 99.8, and 98.2% at frequencies of 6.5, 17.8, and 19.6 GHz, respectively. As shown in Fig. 4c, the third resonator provides absorption efficiencies of 98.3 and 93.7% at frequencies of 12.4 and 19.4 GHz in the Ku- and K-bands, respectively. The fourth resonator exhibits high performance with an absorption rate of 98% at a single frequency of 17.2 GHz in Fig. 4d. The absorption achieved by the fourth resonator is emphasized as a significant advancement, increasing the number of bands in the metasurface-based hepta-band absorber from six to seven. Additionally, the high absorption performance of 99.8% at a frequency of 19.5 GHz is attributed to the integration of the first, second, and third resonators. When comparing the design steps that constitute the proposed absorber with its final configuration, some differences in frequency points and absorption performance percentages are observed. These differences arise from the integration of the resonators and the coupling capacitance between them.

3 Theory and Performance Analysis

3.1 Theory

The mathematical analysis of the absorption phenomenon in absorber designs is expressed as shown in Eq. (1) [47].

$$A(w) = 1 - R(w) - T(w), \tag{1}$$

$A(w)$ represents the absorption coefficient, $R(w) = |S_{11}|^2$ represents the reflection coefficient, and $T(w) = |S_{21}|^2$ represents the transmission coefficient. Since the background is a metal termination, the transmission coefficient approaches zero. In this case, the transmission coefficient can be neglected, and the absorption coefficient is solely related to the reflection coefficient. Therefore, the expression, in Eq. (1), simplifies to $A(w) = 1 - R(w)$ holds true. This article aims to reduce the reflection coefficient of the proposed absorber to approximately zero. Thus, the goal is to ensure that absorption is close to 1, achieving maximum performance for the absorber.

The mathematical expression relating the reflection coefficient to the characteristic impedance is given in Eq. (2) [48]. In this expression, Γ represents the reflection coefficient, Z_{in} represents the input impedance, and Z_0 represents the impedance of free space.

$$\Gamma = \frac{Z_{in} - Z_0}{Z_{in} + Z_0}, \tag{2}$$

To validate the metasurface properties of the proposed absorber, it is essential to accurately calculate the permeability and permittivity values. The Nicolson–Ross–Weir (NRW) method has been preferred for determining these parameters due to its practicality and ease of implementation. Using the NRW method, the parameters that define the electromagnetic properties of the material are expressed through the reflection and transmission parameters, as expressed in Eqs. (3), (4), (5), and (6) [49].

$$\epsilon_r = \frac{2}{jwd}\frac{1-(S_{21+}S_{11})}{1+(S_{21+}S_{11})}, \tag{3}$$

$$\mu_r = \frac{2}{jwd}\frac{1-(S_{21}-S_{11})}{1+(S_{21}-S_{11})}, \tag{4}$$

$$\eta_r = \sqrt{\mu_r \epsilon_r} = \frac{c}{j\pi f d}\sqrt{\frac{(S_{21-}1)^2-(S_{11})^2}{(S_{21}+1)^2-(S_{11})^2}}, \tag{5}$$

$$Z_r = \sqrt{\frac{\mu_r}{\epsilon_r}} = \sqrt{\frac{(1+S_{11})^2-(S_{21})^2}{(1-S_{11})^2-(S_{21})^2}}, \tag{6}$$

In Eqs. (3), (4), (5), and (6), ω represents the angular frequency (rad/s), d is the thickness of the material, S_{11} is the reflection coefficient, f is the frequency (Hz), ε_r is the relative permittivity (F/m), μ_r is the relative permeability (H/m), n_r is the relative refractive index, and Z_r is the relative impedance (Ω).

3.2 Performance Analysis

To gain a better understanding of the physical mechanism of the proposed metasurface absorber, the performance at the resonance frequencies where absorption occurs was analyzed in terms of impedance, permittivity, permeability, angular sensitivity, surface current behavior, and field distributions. Firstly, the impedance behavior of the absorber at its resonance frequencies is investigated in Fig. 5a. Figure 5a presents the graph of the normalized impedance of the proposed absorber within the frequency range of $1-20$ GHz. At the resonance frequencies where absorption occurs, the real parts of the impedance approach one, while the imaginary parts approach zero, thereby matching the impedance of free space. Next, to validate the metamaterial properties of the proposed absorber, the values of permittivity, permeability, and refractive index were calculated using Nicolson–Ross–Weir (NRW) Eqs. (3),(4), and (5). As a result of these calculations, the permittivity, permeability, and refractive index values obtained at each resonance frequency are presented in detail in Table 2. The analysis in Table 2 shows that one of the permittivity and permeability values is negative, while the other is positive, which confirms the presence of MNG (mu negative metamaterial) and ENG (epsilon negative metamaterial) characteristics. Furthermore, the refractive index approaches zero at each resonance frequency, allowing the formation of evanescent waves within the absorber. The results of the dielectric and permeability graphs obtained by integrating the Nicolson–Ross–Weir Eqs. (3) and (4) into MATLAB software are presented in 5b,c [45, 50, 51].

When actions are taken for real-time applications of the design, the angle of incidence for an EM wave is uncertain and requires an analysis of the angular stability of the metasurface at the absorption frequencies. Additionally, literature studies indicate that an effective absorber should perform well over a wide range of incident angles and be insensitive to different polarizations. Figure 6a,b presents the absorption spectra for different incident angles for TE and TM modes, respectively. The analyses were conducted with simulations taken at every 15 degrees within the angle range of 0 to 75 degrees.

In Fig. 6a, it has been concluded that the absorption performance for different incident angles in the TE mode shows over 80% for all peaks except for the third peak up to 45 degrees. Analyzing the peak points where absorption occurs reveals that the first absorption peak is 80%, the second absorption peak is 87.4%, the third absorption peak is 65%, the fourth absorption peak is 90.7%, the fifth absorption peak is 80%, the sixth absorption peak is 94%, and the seventh and final absorption peak demonstrates a performance of 99.2%. The sensitivity of resonance dominance depends on the geometry of the structure and the electromagnetic properties of the material used, leading to the distortion of resonance at oblique angles. Additionally, the variation in electric and magnetic field interactions at different angles weakens the strength of resonance. The coupling effect between resonators also contributes to the weakening of resonance at oblique angles. These factors are observed to have a greater impact on the resonance dominance at the third absorption peak [52]. In Fig. 6b, when the analysis is performed for different incident angles in the TM mode, it is concluded that the absorption performance remains above 80% up to 45 degrees. When analyzing the absorption graphs of the proposed MSA at different incident angles, shifts are observed at certain frequency points. These shifts are attributed to the polarization-dependent interactions of the electric and magnetic fields, as well as diffraction effects.

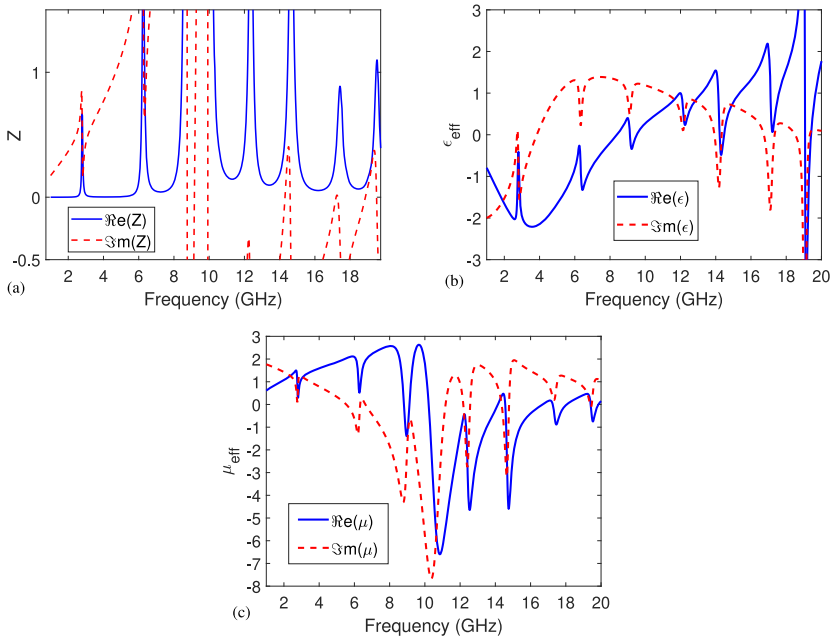

Fig. 5 **a** Normalized impedance, **b** effective permittivity, and **c** effective permeability graphics for the proposed metasurface absorber

Table 2 Values of permittivity, permeability, and refractive index

Absorption frequency	Re(ϵ_r)	Im(ϵ_r)	Re(μ_r)	Im(μ_r)	Re(n)	Im(n)
2.8 GHz	−0.4	−0.9	0.4	0.8	0	0
6.32 GHz	−0.7	0.2	0.7	−0.1	0	0.1
9.17 GHz	−0.3	0.5	0.6	−0.6	0.03	0
12.21 GHz	0.2	0.3	−0.4	−0.3	0	0
14.4 GHz	−0.1	0.5	0.4	−0.2	0	0
17.3 GHz	0.3	−0.09	−0.15	0.2	0.06	0.09
19.5 GHz	0.46	0.12	−0.7	−0.05	0	0.07

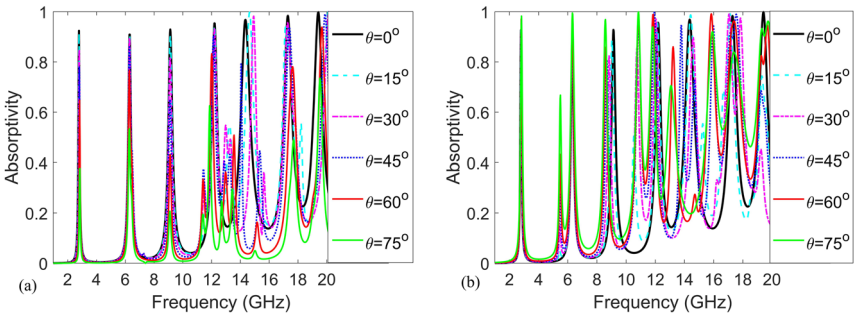

Fig. 6 Effect of different incident angle variations on the absorption spectrum for the proposed MSA in **a** TE and **b** TM modes

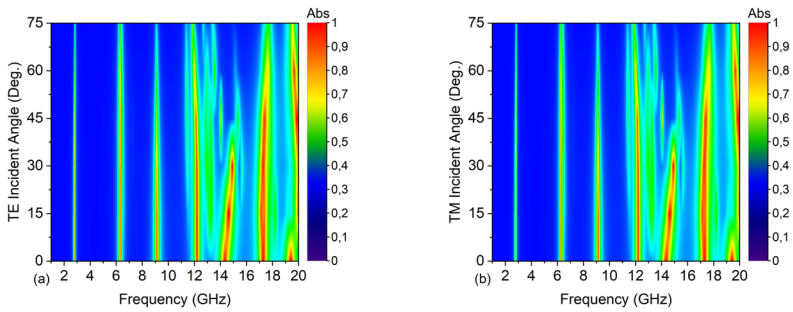

Fig. 7 Effect of polarization angle variations on the absorption spectrum of the proposed MSA in **a** TE and **b** TM modes

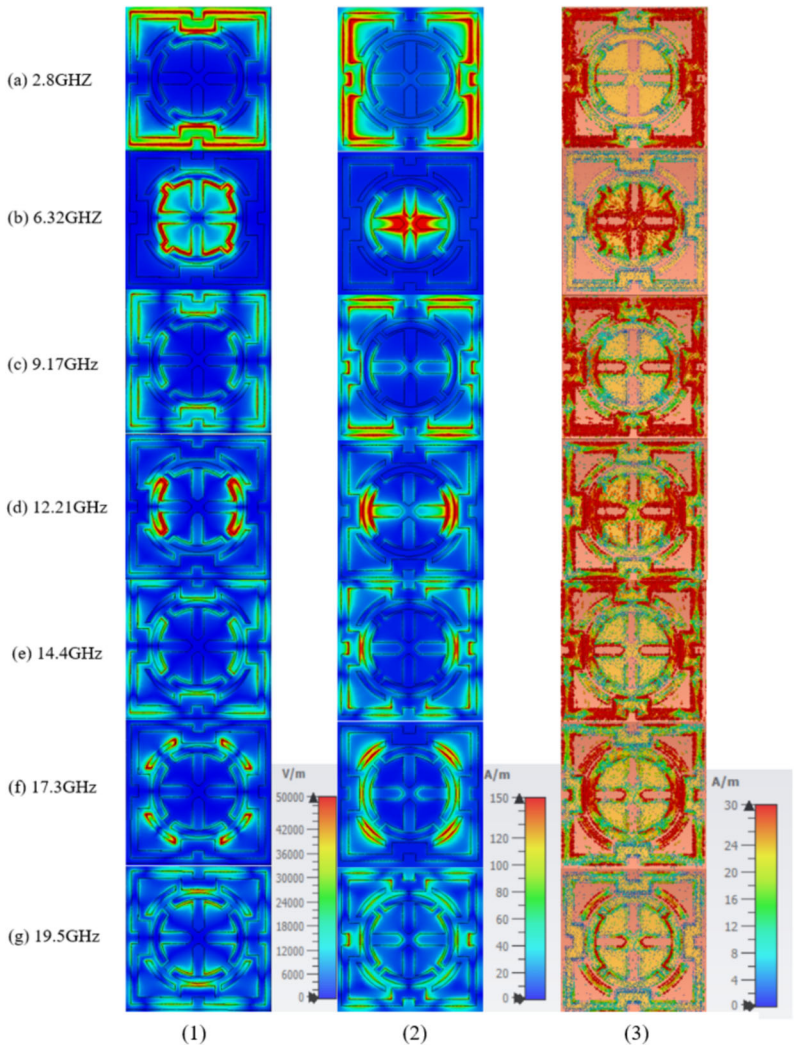

Fig. 8 (1) Electric (E), (2) magnetic (H), and (3) surface current distribution presentations for the proposed MSA

Figure 7a, b shows the effects of polarization angle variations on the absorption spectra in the TE and TM modes, respectively.

The results in Fig. 7a,b show that the proposed absorber exhibits consistent performance, demonstrating polarization-insensitive behavior in both TE and TM modes, unaffected by variations in the polarization angle. As seen in Fig. 7a,b, the proposed design demonstrates an absorption performance of over 80% for both TE and TM polarization up to 45 degrees, except for the third peak. When Fig. 7a,b is examined, it can be observed that at normal incidence, the absorption remains above 80% up to 60 degrees for the 4th, 5th, 6th, and 7th peaks, where absorption is high. The proposed metasurface absorber demonstrates the same performance under normal incidence for both TE and TM modes, making it particularly efficient for applications that require polarization sensitivity [53].

In Fig. 8(1-2-3), the electrical, magnetic, and surface field distributions of the proposed metasurface-based absorber are examined at frequencies of in Fig. 8(1-2-3)(a) 2.8, Fig. 8(1-2-3)(b) 6.32, Fig. 8(1-2-3)(c) 9.17, Fig. 8(1-2-3)(d) 12.21, Fig. 8(1-2-3)(e) 14.4, Fig. 8(1-2-3)(f) 17.3, and Fig. 8(1-2-3)(g) 19.5 GHz to better understand the absorption mechanism and validate the effects of the resonators on the frequency bands. At a frequency of 2.8 GHz, the electric field is concentrated at the upper and lower parts of the square frame of the first resonator, while the surface currents create an antiparallel flow, circulating clockwise on the right side of the protruding outer square and counterclockwise on the left side. At 6.32 GHz, a significant increase in the electric field is observed in the outer regions of the circular structure of the second resonator, with surface currents flowing clockwise on the right side and counterclockwise on the left side of the inner surface of the second resonator. At 12.21 GHz, in the slotted ring of the third resonator, the electric field is concentrated on the right and left sides, with current flowing counterclockwise on the right and clockwise on the left. At a frequency of 14.4 GHz, the electric field reaches a high concentration at the upper and lower parts of the protrusions of the first resonator, with the current direction flowing upward

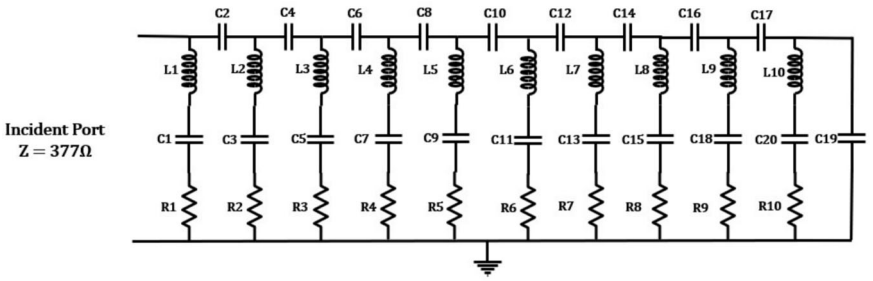

Fig. 9 ECM of the proposed hepta-band metasurface absorber

Table 3 Values of corresponding electronic components

Resistance (Ω)	Series capacitance (fF)	Parallel capacitance (fF)	Inductance (nH)
R1=234.506	C1=20.5836	C2=32.6912	L1=163.96
R2=0.107503	C3=3626.6	C4=17749.5	L2=1.45808
R3=3456.73	C5=26.1828	C6=21394.7	L3=22.3995
R4=28.2077	C7=27.7847	C8=784.428	L4=8.38011
R5=9.63747	C9=8.91515	C10=653.342	L5=11.9289
R6=3.01713	C11=4.6754	C12=451.501	L6=15.9811
R7=6.36665	C13=24.5904	C14=366.256	L7=6.81074
R8=36.7424	C15=120.473	C16=1940.06	L8=7.50434
R9=35.3775	C17=9.94992	C18=93.2629	L9=6376.74
R10=36.9289	C19=67.4036	C20=13.6784	L10=10.0918

on the right protrusion and downward on the left protrusion. At 17.3 GHz, the interaction of the electric field intensities in the fourth and second resonators results in a high absorption performance of 98.3%. At 19.5 GHz, the simultaneous increase in the electric field intensities of the first, second, and third resonators indicates that absorption occurs due to the integrated effect of these resonators.

To validate the absorption characteristics of the proposed metasurface absorber, an equivalent circuit model (ECM) for the designed unit cell was developed using lumped elements and simulated with the ADS circuit simulator. This model is presented in Fig. 9. The equivalent circuit model of the unit cell of the proposed hepta-band metasurface absorber is represented by RLC resonators, which are responsible for the formation of each resonance frequency. The resistive elements (R_1, R_2, R_3, R_4, R_5, R_6, R_7, R_8, R_9, R_{10}) in the equivalent circuit increase energy losses by converting the energy of electromagnetic waves into heat. The series capacitors ($C_1, C_3, C_5, C_7, C_9, C_{11}, C_{13}, C_{15}, C_{17}, C_{19}$) determine the resonance frequencies of the circuit while serving to store electric field energy, while the inductors (L_1, L_2, L_3, L_4, L_5, L_6, L_7, L_8, L_9, L_{10}) serve to store magnetic energy at the resonance frequencies [54]. To obtain the S_{11} parameter of the proposed metasurface absorber, the values of all circuit elements were optimized using the ADS program, and these values are presented in Table 3. In Fig. 10, the S11 values obtained from both ADS and CST Microwave Studio software are compared. For the resonance frequencies, it was observed that the S_{11} values from both software tools matched consistently, which supports the accuracy and validity of the design approach.

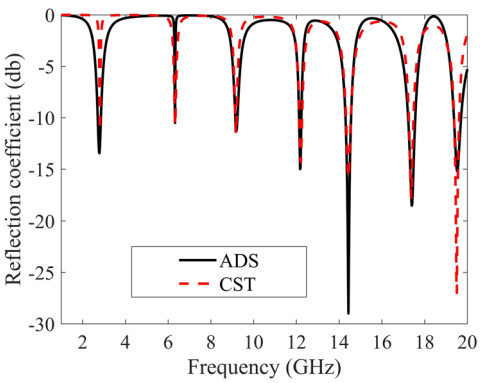

Fig. 10 S_{11} simulation results obtained using ADS and CST for the proposed hepta-band MSA

3.3 Parametric Structural Analysis

The critical parameter selection for the optimal operation of the proposed metasurface absorber was performed through a parameter sweep. For this purpose, the variation in absorption performance was investigated by changing the parameters l_2, r_3, r_5, and w_3 within the ranges of [14;15.3], [5.5;7.3],

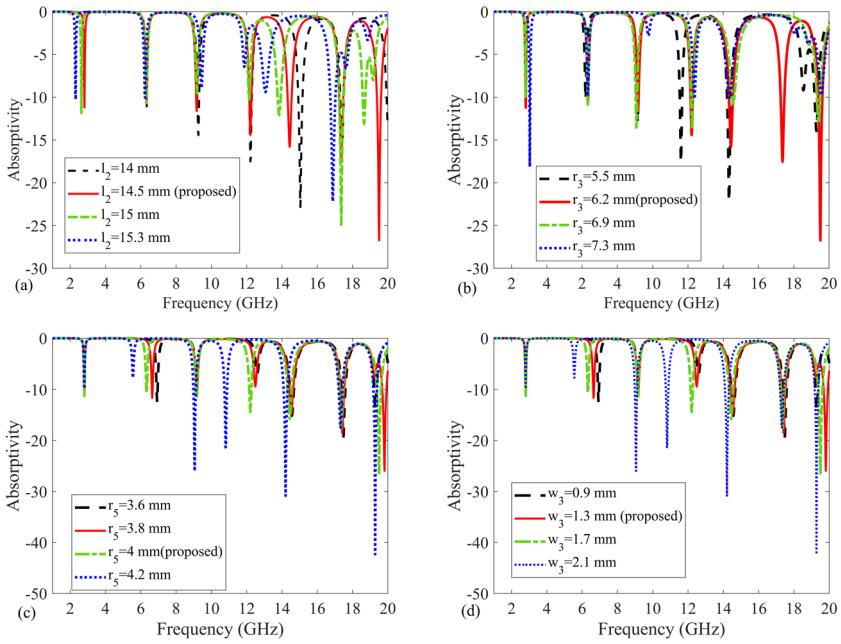

Fig. 11 Effect of the proposed MSA's **a** l_2, **b** r_3, **c** r_5, and **d** w_3 parameters on the absorption spectrum

[3.6;4.2] and [0.9;2.1], respectively. The absorption performances corresponding to these parameter variations are presented in Fig. 11a–d. As shown in Fig. 11a–d, the strongest absorption performance was achieved when $l_2 = 14.5$ mm, $r_3 = 6.2$ mm, $r_5 = 4$ mm, and $w_3 = 1.3$ mm.

3.4 RCS Reduction Performance and Scaling

As a significant advantage of the proposed metasurface absorber over existing designs, we have demonstrated its capability for radar cross section (RCS) reduction. This application provides a notable advantage compared to existing designs. To this end, the monostatic RCS reduction potential was investigated for a sample produced with a 13x13 unit cell, and it was proved that it operates with an RCS reduction of at least 7 dBsm at the absorbing frequencies. For the 13x13 metasurface absorber shown in Fig. 12a, the calculation of the monostatic RCS reduction value was simulated. To achieve this, the RCS of the metasurface shown in Fig. 12a and the RCS of the PEC selected as a reference were calculated as shown in Fig. 12b. The RCS reduction value against the selected reference PEC is presented in Fig. 12c. As shown in Fig. 12c, the RCS reduction value is above 5 dBsm at all frequencies where absorption occurs. Therefore, the produced sample offers significant advantages in radar application usage [55]. Additionally, as a supplementary feature, we scaled the proposed design by a factor of 1.66 and demonstrated its similar absorption performance in the L-, S-, C-, and X-bands, as shown in Fig. 12d. As illustrated in Fig. 12d, the scaled absorber achieves absorption rates of 92.6%, 91.7%, 93%, 96.3%, 97.4%, 98.3%, and 99.8% at frequencies of 1.68 GHz, 3.79 GHz, 5.52 GHz, 7.3 GHz, 8.7 GHz, 10.52 GHz, and 11.85 GHz, respectively [56].

3.5 Experimental Results

To validate the simulation results of the proposed metasurface absorber, real-time measurements were conducted. Initially, the prototype of the metasurface-based absorber, consisting of $13x13$ unit cells as shown in Fig. 13a, was fabricated using conventional PCB printing techniques. Subsequently, free space reflection measurements were performed with the measurement setup illustrated in Fig. 13b under anechoic chamber conditions. In this setup, two horn antennas operating in the frequency range of $1-18$ GHz were connected to a Keysight N9923A vector network analyzer (VNA), creating a transmission line path. The calibration of the transmission line was conducted using the TRL (Through-Reflect-Line) calibration method. Prior to the measurements, the network analyzer was calibrated. After completing the calibration step, the produced prototype was placed in front of the horn antennas, and the reflection coefficient was then measured.

In Fig. 13a, the manufactured form of the proposed metasurface absorber consisting of a $13x13$ unit cell is presented. Figure 13b shows the measurement setup for the proposed metasurface absorber. As indicated in Fig. 13b, the measurement results obtained under anechoic chamber conditions are provided in Fig. 13c. As seen in Fig. 13c, the simulation and measurement results are nearly in perfect agreement. When comparing the experimental and simulated results, consistent outcomes have been obtained with minor differences. The reasons for these small discrepancies may include potential

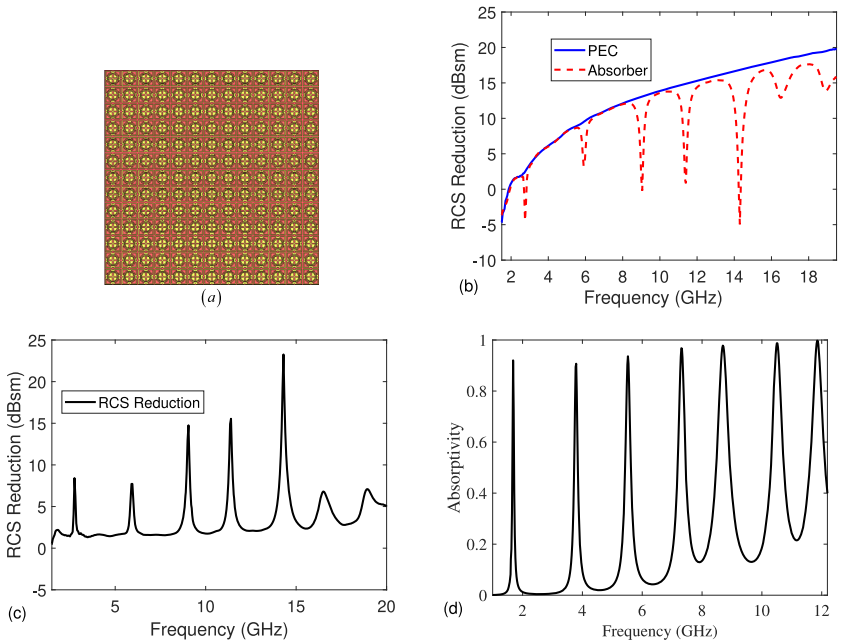

Fig. 12 Proposed MSA's **a** 13x13 unit cell, **b** RCS of metasurface, **c** RCS reduction on the absorption spectrum, and **d** 1.6 scaling absorber performance

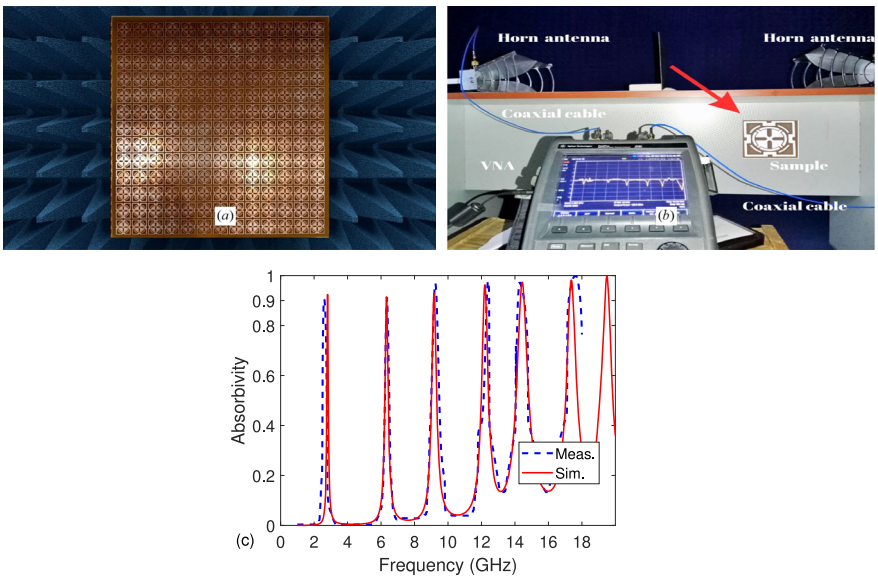

Fig. 13 **a** Fabricated metamaterial sample, **b** schematic view of measurement setup, **c** experimental and numerical reflection coefficient results

errors during the manufacturing process, alignment issues during measurements, the conditions of the anechoic chamber where the measurements were conducted, and effects such as reflections. In addition, unlike the application of infinite boundary conditions in the simulation the use of a 13x13 unit cell sample in the real measurement scenario, manual measurements, and calibration errors are the reasons for this discrepancy[57–59].

4 Comparison

To analyze the performance of the proposed metasurface absorber, a comparison was made with similar studies in the literature. Table 4 presents a comparison of the performance of the proposed work with that of similar studies. In Table 4, the absorption rates are compared according to resonator frequencies (Res. freq.- Absorp. (GHz- %)), the number of

Table 4 Comparison of the proposed hepta-band MSA with other reported absorber designs

Refs.	Res. freq.- Absorp	N.B	Operating freq	Thickness	Substrate	Obliq
Ref. [42]	21.4(99.9), 24.4(96) and 27.8(99.4)	3	K-Ka	$\lambda = 0.109\lambda_0$ 1.54mm	FR-4	45^o
Ref. [43]	3.64(91.46), 5.99(99.72), 7.47(96.89) and 10.01(98.45)	4	S-C-X	$\lambda = 0.019\lambda_0$ 1.6mm	FR-4	Unspecified
Ref. [44]	2.57(92.87), 5.64(76.9) 8.32(94.12) and 13.45(90.97)	4	S-C-X Ku	$\lambda = 0.013\lambda_0$ 1.6mm	FR-4	90^o
Ref. [60]	2.248(96), 2.878(93), 4.3(93) and 5.872(95)	4	S-C	$\lambda = 0.011\lambda_0$ 1.5mm	FR-4	45^o
Ref. [61]	4.1(97.9), 6.86(99.1), 11.3(99.5) and 13.45(99.95)	4	C-X-Ku	$\lambda = 0.02\lambda_0$ 1.5mm	FR-4	Unspecified
Ref. [62]	3.55(99.75), 5.15(99.96) 10.12(99.91), 12.52(99.93) 15.90(98.79) and 21.97(94.45)	6	S-C-X Ku-K	$\lambda = 0.012\lambda_0$ 1mm	FR-4	90^o
Ref. [63]	10.4(99.9), 12.80(98.44) 21,05(86,78), 24.29(92.74) and 30.41(93.65)	5	X-Ku-K Ka	$\lambda = 0.03\lambda_0$ 1mm	FR-4	Unspecified
Ref. [64]	5,026(95.67), 8,582(99.16) 11,73(95.97) and 15,036(97.02)	4	C-X-Ku	$\lambda = 0.0134\lambda_0$ 0.8mm	FR-4	$TE = 30^o$ $TM = 60^o$
Ref. [65]	4,70(90.89), 10,19(90.18) 11,96(94.80) and 14,15(90)	4	C-X-Ku	$\lambda = 0.013\lambda_0$ 0.83mm	Polyimide	45^o
Ref. [66]	4.59(97), 6.84(78), 9.35(92) 13.60(99) and 16.08(95)	5	C-X-Ku	$\lambda = 0.024\lambda_0$ 1.57mm	FR-4	90^o
Ref. [67]	3.02(99.86), 5.71(97.58) and 8.36(97.46)	3	S-C-X	$\lambda = 0.016\lambda_0$ 1.6mm	FR-4	75^o
Ref. [68]	3.26(93.8), 11.6(96.47) and 17.13(99.95)	3	S-X-Ku	$\lambda = 0.017\lambda_0$ 1.6mm	FR-4	60^o
Ref. [45]	3.15(93.65), 5.96(85.75), 8.73(94.14) 9.36(99.51), 13.22(90.55), 13.71(97.87) and 14.45(98.68)	7	S-C-X Ku	$\lambda = 0.0168\lambda_0$ 1.6mm	FR-4	50^o
Ref. [69]	5.2(99.7), 8.65(99.8), 9.63(98.8) 13.53(99.9), 14.5(99.7), 16.6(99.9) and 18.92(99.8)	7	C-X-Ku-K	$\lambda = 0.0277\lambda_0$ 1.6mm	FR-4	$TE = 60^o$ $TM = 70^o$
This Paper	2.33(90.75), 6.17(92.06), 9.85(94.83) 11.43(94.53), 13.69(98.67), 17.94(98.61) and 18.78(99.79)	7	S-C-X Ku-K	$\lambda = 0.0093\lambda_0$ 1mm	FR-4	45^o

microwave bands absorbed (N.B.), the operating microwave band (Operating freq.), thickness, substrate, and angle sensitivity (Obliq. Ang.).

When examining Table 4, it can be observed that the proposed design achieves absorption in seven bands, while most of the other studies [42–44, 60–68] provide absorption in a maximum of six bands. Additionally, while most similar studies [42–45, 60, 61, 63–69] operate effectively in a maximum of four microwave bands, the proposed design is active in five microwave bands (S, C, X, Ku, and K). Despite the ultra-thin of the metasurface substrate and the use of the high dielectric FR4 material, a superior metasurface absorber geometry has been chosen, resulting in higher efficiency compared to other studies. Analyzing Table 4 in terms of thickness in wavelengths, the proposed absorber is noted to be thinner compared to other studies [42–45, 60–69]. Furthermore, from an economic perspective, it is produced from inexpensive and available materials. Additionally, the compatibility of the FR-4 material with existing PCB manufacturing technologies makes the design and prototyping processes faster and more efficient compared to other stud-

ies [65]. Finally, it demonstrates sufficient sensitivity to meet the requirements for oblique angle performance.

5 Conclusion

In this study, a metasurface-based absorber has been designed for S-, C-, X-, Ku-, and K-band microwave frequencies. The absorber achieves over 90% absorption efficiency across seven bands and is fabricated using a low-cost FR-4 substrate material with a thickness of 1 mm ($0.0093\lambda_0$). Due to its symmetric structure, the absorber operates with polarization insensitivity and demonstrates more than 80% performance at oblique angles up to 45 degrees. Additionally, the equivalent circuit model (ECM) of the unit cell structure was simulated using the ADS simulator and validated by comparing the results with those obtained from CST software. For real-time validation, a prototype was fabricated, and measurements showed good agreement with the simulation results.

Funding Open access funding provided by the Scientific and Technological Research Council of Türkiye (TÜBİTAK).

References

1. Shukoor, M.A.; Dey, S.; Koul, S.K.: Broadband polarization insensitive wide angular stable dual-split square ring circuit analog absorber for radar cross section and electromagnetic interference shielding applications. Int. J. RF Microwave Comput. Aided Eng. **32**(5), 23085 (2022)
2. Wang, Y.; Cui, Z.; Zhu, D.; Yue, L.: Composite metamaterials for thz perfect absorption. Physica status solidi (a) **216**(6), 1800940 (2019)
3. Omoru, E.O.; Srivastava, V.M.: Mosfet based absorber for reflected signal in 5g massive mimo base station-a circuit perspective. J. Commun. **15**(11), 833–840 (2020)
4. Lv, Q.; Chen, Y.; Yu, S.; Zhou, X.; Wei, Y.; Li, L.; Wang, J.; Li, B.: Quad-band bidirectional metasurface microwave absorber with a patchwork of circular-patch resonators. Mater. Today Commun. **38**, 108336 (2024)
5. Ozturk, G.; Hasar, U.C.; Ertugrul, M.; Tutar, F.; Corapsiz, M.F.; Kurt, M.; Donmez, K.; Ismail, I.; Alfaqawi, M.S.: An efficient cost effective wide-angle metasurface-based linear and circular polarization converter for x-, ku-and k-band applications. Opt. Laser Technol. **163**, 109404 (2023)
6. Deng, G.; Zhu, Y.; Zhang, Q.; Zhang, G.; Yin, Z.; Yang, J.; Li, Y.: Reconfigurable linear-to-circular polarization conversion using liquid crystal-based reflective metasurface. IEEE Antennas Wirel. Propag. Lett. **23**(7), 2249–2253 (2024)
7. Awan, W.A.; Hussain, N.; Park, S.G.; Kim, N.: Intelligent metasurface based antenna with pattern and beam reconfigurability for internet of things applications. Alex. Eng. J. **92**, 50–62 (2024)
8. Li, S.; Ma, B.; Li, Q.; Rybin, M.V.: Antenna-based approach to fine control of supercavity mode quality factor in metasurfaces. Nano Lett. **23**(14), 6399–6405 (2023)
9. Saxena, G.; Chintakindi, S.; Vennu, V.; Abidi, M.H.; Saif, W.A.M.; Maduri, P.K.; Singh, H.; Awasthi, Y.K.: Tunable wideband cylindrical dielectric resonator inspired metasurface absorber for medical sensing applications (2023)
10. Lin, X.; Chen, Y.; Gong, Z.; Seet, B.-C.; Huang, L.; Lu, Y.: Ultrawideband textile antenna for wearable microwave medical imaging applications. IEEE Trans. Antennas Propag. **68**(6), 4238–4249 (2020)
11. Shukoor, M.A.; Dey, S.: Compact, broadband, wide angular stable circuit analog absorber at sub-6 ghz for radar cross section reduction. Microw. Opt. Technol. Lett. **63**(12), 2938–2943 (2021)
12. Ajaikumar, V.; Jose, K.; Mohanan, P.; Nair, K.: Reduction of radar cross section of corner reflectors using strip grating technique. In: IEEE Antennas and Propagation Society International Symposium 1992 Digest, pp. 707-710 (1992). IEEE
13. Wang, Z.; Hu, G.; Wang, X.; Ding, X.; Zhang, K.; Li, H.; Burokur, S.N.; Wu, Q.; Liu, J.; Tan, J.; et al.: Single-layer spatial analog meta-processor for imaging processing. Nat. Commun. **13**(1), 2188 (2022)
14. Zhang, X.; Zhou, Y.; Zheng, H.; Linares, A.E.; Ugwu, F.C.; Li, D.; Sun, H.-B.; Bai, B.; Valentine, J.G.: Reconfigurable metasurface for image processing. Nano Lett. **21**(20), 8715–8722 (2021)
15. Yang, H.; Feng, Q.; Wang, X.; Urynbassarova, D.; Teali, A.A.: Reduced biquaternion windowed linear canonical transform: properties and applications. Mathematics **12**(5), 743 (2024)
16. Mohanty, A.; Acharya, O.P.; Appasani, B.; Mohapatra, S.; Khan, M.S.: Design of a novel terahertz metamaterial absorber for sensing applications. IEEE Sens. J. **21**(20), 22688–22694 (2021)
17. Singh, H.; Gupta, A.; Kaler, R.S.; Singh, S.; Gill, A.S.: Designing and analysis of ultrathin metamaterial absorber for w band biomedical sensing application. IEEE Sens. J. **22**(11), 10524–10531 (2022)
18. Yao, Y.; Shu, F.; Cheng, X.; Liu, H.; Miao, P.; Wu, L.: Automotive radar optimization design in a spectrally crowded v2i communication environment. IEEE Trans. Intell. Transp. Syst. **24**(8), 8253–8263 (2023)
19. Tian, R.; Guan, H.; Lu, X.; Zhang, X.; Hao, H.; Feng, W.; Zhang, G.: Dynamic crushing behavior and energy absorption of hybrid auxetic metamaterial inspired by islamic motif art. Appl. Math. Mech. **44**(3), 345–362 (2023)
20. Zhang, X.; Zhang, H.; Liu, L.; Han, Z.; Poor, H.V.; Di, B.: Target detection and positioning aided by reconfigurable surfaces: Reflective or holographic. IEEE Trans. Wireless Commun. **23**(12), 19215–19230 (2024)
21. Wang, Y.; Xiao, R.; Xiao, N.; Wang, Z.; Chen, L.; Wen, Y.; Li, P.: Wireless multiferroic memristor with coupled giant impedance and artificial synapse application. Adv. Electron. Mater. **8**(10), 2200370 (2022)
22. Kim, Y.; Lee, J.-H.: Broadband metasurface absorber based on an optimal combination of copper tiles and chip resistors. Materials **16**(7), 2692 (2023)
23. Persis, G.E.; Paul, J.J.; Mary, T.B.; Joy, R.C.: A compact tilted split ring multiband metamaterial absorber for energy harvesting applications. Mater. Today: Proc. **56**, 368–372 (2022)

24. Jahan, M.I.; Ullah, M.; Ahmad, H.; Roslan, R.; Misnon, I.I.; Jose, R.: Two split rings resonator-based perfect metamaterial absorbers with the incident and polarization angle independent for sensing applications. J. Magn. Magn. Mater. **594**, 171904 (2024)
25. Li, Y.; Gao, W.; Guo, L.; Chen, Z.; Li, C.; Zhang, H.; Jiao, J.; An, B.: Tunable ultra-broadband terahertz perfect absorber based on vanadium oxide metamaterial. Opt. Express **29**(25), 41222–41233 (2021)
26. Liu, Y.; Qian, Y.; Hu, F.; Jiang, M.; Zhang, L.: A dynamically adjustable broadband terahertz absorber based on a vanadium dioxide hybrid metamaterial. Res. Phys. **19**, 103384 (2020)
27. Wen, P.; Jiang, Y.; Liu, F.; Ma, Z.; Wang, Y.: Direct synthesis of continuously tunable wideband bandpass filtering attenuator with multiple transmission zeros. IEEE Transactions on Circuits and Systems II: Express Briefs (2024)
28. Yu, S.; Guan, D.; Gu, Z.; Guo, J.; Liu, Z.; Liu, Y.: Radar target complex highresolution range profile modulation by external time coding metasurface. IEEE Trans. Microw. Theory Tech. **72**(10), 6083–6093 (2024)
29. Kanjanasit, K.; Tantipiriyakul, T.; Wang, C.: Thin film resonant metasurface absorbers using patch-based arrays on liquid crystal polymer substrates for centimeter-wave applications. Heliyon **10**(15), e35399 (2024)
30. Afsar, M.; Faruque, M.; Hossain, M.B.: Holy cross-moon shaped dual band perfect metamaterial absorber for c-band application. Mater. Today Commun. **33**, 104309 (2022)
31. Choudhary, A.; Pal, S.; Sarkhel, G.: Broadband millimeter-wave absorbers: a review. Int. J. Microw. Wirel. Technol. **15**(2), 347–363 (2023)
32. Lv, X.; Withayachumnankul, W.; Fumeaux, C.: Single-fss-layer absorber with improved bandwidth-thickness tradeoff adopting impedance-matching superstrate. IEEE Antennas Wirel. Propag. Lett. **18**(5), 916–920 (2019)
33. Cai, W.; Liu, P.; Wang, Q.; Zhang, Q.; Pang, X.; Men, W.: A double layer coupled broadband absorbing metamaterial with optical transparency characteristics. In:2023 International Applied Computational Electromagnetics Society Symposium (ACES-China), pp. 1-3 (2023). IEEE
34. Ren, Z.; Lin, Z.; Zhi, X.; Li, M.: Double-layer broadband perfect metamaterial absorber and its potential for refractive index sensing. Opt. Mater. **99**, 109575 (2020)
35. Li, L.; Ruan, H.; Liu, C.; Li, Y.; Shuang, Y.; Alù, A.; Qiu, C.-W.; Cui, T.J.: Machine-learning reprogrammable metasurface imager. Nat. Commun. **10**(1), 1082 (2019)
36. Dai, J.Y.; Tang, W.; Yang, L.X.; Li, X.; Chen, M.Z.; Ke, J.C.; Cheng, Q.; Jin, S.; Cui, T.J.: Realization of multi-modulation schemes for wireless communication by time-domain digital coding metasurface. IEEE Trans. Antennas Propag. **68**(3), 1618–1627 (2019)
37. Katrodiya, D.; Jani, C.; Sorathiya, V.; Patel, S.K.: Metasurface based broadband solar absorber. Opt. Mater. **89**, 34–41 (2019)
38. Landy, N.I.; Sajuyigbe, S.; Mock, J.J.; Smith, D.R.; Padilla, W.J.: Perfect metamaterial absorber. Phys. Rev. Lett. **100**(20), 207402 (2008)
39. Hannan, S.; Islam, M.T.; Sahar, N.M.; Mat, K.; Chowdhury, M.E.; Rmili, H.: Modified-segmented split-ring based polarization and angle-insensitive multiband metamaterial absorber for x, ku and k band applications. IEEE Access **8**, 144051–144063 (2020)
40. Elakkiya, A.; Radha, S.; Sreeja, B.; Manikandan, E.: An ultrathin microwave metamaterial absorber for c, x, and ku band applications. J. Electron. Mater. **50**, 7275–7282 (2021)
41. Yousaf, A.; Murtaza, M.; Wakeel, A.; Anjum, S.: A highly efficient low-profile tetra-band metasurface absorber for x, ku, and k band applications. AEUInt. J. Electron. Commun. **154**, 154329 (2022)
42. Dewangan, L.; Patinavalasa, M.S.; Acharjee, J.; Solunke, Y.; Ghosh, S.; Mishra, N.K.: Broadband metamaterial absorber for stealth applications at k-band. AEUInt. J. Electron. Commun. **170**, 154828 (2023)
43. Rabbani, M.G.; Islam, M.T.; Hoque, A.; Bais, B.; Albadran, S.; Islam, M.S.; Soliman, M.S.: Orthogonal centre ring field optimization triple-band metamaterial absorber with sensing application. Eng. Sci. Technol., Int. J. **49**, 101588 (2024)
44. Hasan, M.S.; Islam, M.T.; Samsuzzaman, M.; Alamri, S.; Albadran, S.; Moniruzzaman, M.; Soliman, M.S.: Double elliptical resonator based quad-band incident angle and polarization angle insensitive metamaterial absorber for wireless applications. Opt. Laser Technol. **171**, 110334 (2024)
45. Errajraji, K.; Jebbor, N.; Das, S.; Islam, T.; Madhav, B.; El-Arrouch, T.: Design and analysis of a multi-band miniaturized metamaterial absorber for wireless communication applications. Opt. Quant. Electron. **56**(2), 232 (2024)
46. Jackson, J.D.: Classical Electrodynamics. John Wiley Sons, Hoboken (2021)
47. Shen, X.; Cui, T.J.; Zhao, J.; Ma, H.F.; Jiang, W.X.; Li, H.: Polarization-independent wide-angle triple-band metamaterial absorber. Opt. Express **19**(10), 9401–9407 (2011)
48. Balanis, C.A.: Advanced Engineering Electromagnetics. John Wiley Sons, Hoboken (2012)
49. Ziolkowski, R.W.: Design, fabrication, and testing of double negative metamaterials. IEEE Trans. Antennas Propag. **51**(7), 1516–1529 (2003)
50. Srinivas, C.; Praveen, K.N.; Kumar, E.R.; Rao, T.C.; Prajapat, C.; Meena, S.S.; Bhatt, P.; Arun, B.; Raju, K.J.; Sastry, D.: Shielding performance of mnxni0. 8-xzn0. 2fe2o4 (0.1 x 0.7) for electromagnetic interference (emi) in x-band frequency. Ceram. Int. **48**(7), 9987–9997 (2022)
51. Srinivas, C.; Praveen, K.N.; Kumar, E.R.; Singh, S.; Meena, S.S.; Bhatt, P.; Rao, T.C.; Sarkar, D.; Arun, B.; Raju, K.J.; et al.: Microwave absorption properties of rare earth (re) ions doped mn-ni-zn nanoferrites (re= dy, sm, ce, er) to shield electromagnetic interference (emi) in x-band frequency. Ceram. Int. **48**(22), 33891–33900 (2022)
52. Chaurasiya, D.; Ghosh, S.; Bhattacharyya, S.; Bhattacharya, A.; Srivastava, K.V.: Compact multi-band polarisation-insensitive metamaterial absorber. IET Microw., Antennas Propag. **10**(1), 94–101 (2016)
53. Hannan, S.; Islam, M.T.; Soliman, M.S.; Faruque, M.; Misran, N.; Islam, M.S.: A co-polarization-insensitive metamaterial absorber for 5g n78 mobile devices at 3.5 ghz to reduce the specific absorption rate. Sci. Rep. **12**(1), 11193 (2022)
54. Hannan, S.; Islam, M.T.; Almalki, S.H.; Faruque, M.; Islam, M.S.: Rotational symmetry engineered, polarization and incident angle-insensitive, perfect metamaterial absorber for x and ku band wireless applications. Sci. Rep. **12**(1), 3740 (2022)
55. Ni, H.; Zhu, Q.; Hua, B.; Mao, K.; Pan, Y.; Ali, F.; Zhong, W.; Chen, X.: Path loss and shadowing for uav-to-ground uwb channels incorporating the effects of builtup areas and airframe. IEEE Trans. Intell. Transp. Syst. **25**(11), 17066–17077 (2024)
56. Li, M.; Wang, T.; Chu, F.; Han, Q.; Qin, Z.; Zuo, M.J.: Scaling-basis chirplet transform. IEEE Trans. Industr. Electron. **68**(9), 8777–8788 (2020)
57. Tutar, F.; Ozturk, G.: An effective metasurface-based linear and circular polarization converter for c-and x-band applications. Opt. Mater. **128**, 112355 (2022)
58. Alahmed Albasry, F.; Ozturk, G.; Hasar, U.C.; Corapsiz, M.F.: Ultra-thin metasurface polarization converter with linear and circular polarization features for rcs applications. Arab. J. Sci. Eng. (2024). https://doi.org/10.1007/s13369-024-09358-y
59. Ozturk, G.; Corapsiz, M.F.: Ultra-thin reflective linear and circular polarization converter for ku band applications. Opt. Commun. **516**, 128268 (2022)

60. Edries, M.; Mohamed, H.A.; Hekal, S.S.; El-Morsy, M.A.; Mansour, H.A.: A new compact quad-band metamaterial absorber using interlaced i/square resonators: design, fabrication, and characterization. IEEE Access **8**, 143723–143733 (2020)
61. Moniruzzaman, M.; Islam, M.T.; Muhammad, G.; Singh, M.; Samsuzzaman, M.: Quad band metamaterial absorber based on asymmetric circular split ring resonator for multiband microwave applications. Res. Phys. **19**, 103467 (2020)
62. Yang, X.; Zhang, X.; Ding, Z.; Zhang, Z.: Compact and ultra-thin absorber based on metasurface for multi-band energy absorption. Optik **273**, 170478 (2023)
63. Verma, A.; Meena, O.P.: Design and analysis of a compact ultrathin penta-band metamaterial absorber. Sadhana **48**(4), 285 (2023)
64. Binda, P.; Singh, R.K.; Mitharwal, R.: An ultra-thin, polarization free wideangle stable quad-band metamaterial absorber for applications in c, x, and ku bands. AEU-Int. J. Electron. Commun. **171**, 154925 (2023)
65. Jin, S.; Zu, H.; Qian, W.; Luo, K.; Xiao, Y.; Song, R.; Xiong, B.: A quad-band and polarization-insensitive metamaterial absorber with a low profile based on graphene-assembled film. Materials **16**(11), 4178 (2023)
66. Ranjan, S.K.; Sahoo, S.: Hexagon enclosed modified g-shaped polarization and incident angle independent metamaterial absorber for s, c, x and ku band frequency. AEU-Int. J. Electron. Commun. **183**, 155348 (2024)
67. Afsar, M.; Faruque, M.; Abdullah, S.; Hossain, M.J.: Rotational symmetric solar system shaped triple band perfect metamaterial absorber for s-, c-, and x-band application. Sens. Actuators, A **365**, 114839 (2024)
68. Rabbani, M.G.; Islam, M.T.; Moniruzzaman, M.; Alamri, S.; Rahman, A.; Moubark, A.M.; Islam, M.S.; Soliman, M.S.: Dumbbell shaped structure loaded modified circular ring resonator based perfect metamaterial absorber for s, x and ku band microwave sensing applications. Sci. Rep. **14**(1), 5588 (2024)
69. Pati, S.S.; Sahoo, S.: Metamaterial-based angular stable polarization-insensitive hepta-band microwave absorber with salient features for rcs reduction and antenna radiation improvement. IEEE Trans. Electromagn. Compat. **66**(3), 761–775 (2024)